EDGE ARTICLE

Check for updates

All publication charges for this article have been paid for by the Royal Society of Chemistry

Cellular delivery of dinucleotides by conjugation with small molecules: targeting translation initiation for anticancer applications†

Natalia Kleczewska, [iD] ‡[a] Pawel J. Sikorski,‡[a] Zofia Warminska,[ab] Lukasz Markiewicz,[a] Renata Kasprzyk, [iD] [abc] Natalia Baran,[ad] Karina Kwapiszewska, [iD] [e] Aneta Karpinska, [iD] [e] Jaroslaw Michalski,[e] Robert Holyst,[e] Joanna Kowalska [iD] *[c] and Jacek Jemielity [iD] *[a]

Targeting cap-dependent translation initiation is one of the experimental approaches that could lead to the development of novel anti-cancer therapies. Synthetic dinucleoside 5′,5′-triphosphates cap analogs are potent antagonists of eukaryotic translation initiation factor 4E (eIF4E) *in vitro* and could counteract elevated levels of eIF4E in cancer cells; however, transformation of these compounds into therapeutic agents remains challenging – they do not easily penetrate into cells and are susceptible to enzymatic cleavage. Here, we tested the potential of several small molecule ligands – folic acid, biotin, glucose, and cholesterol – to deliver both hydrolyzable and cleavage-resistant cap analogs into cells. A broad structure–activity relationship (SAR) study using model fluorescent probes and cap–ligand conjugates showed that cholesterol greatly facilitates uptake of cap analogs without disturbing the interactions with eIF4E. The most potent cholesterol conjugate identified showed apoptosis-mediated cytotoxicity towards cancer cells.

Introduction

Nucleoside and dinucleoside oligophosphates, and their synthetic analogs, are a class of biologically active compounds which often act as modulators of metabolic pathways and protein activity in cells and, therefore, have great therapeutic potential.[1] However, *in vivo* applications of these compounds are largely limited due to poor cellular permeability arising from high polarity and a negative net charge at physiological pH.[2] To date, the cell-permeability issue for nucleotides has been fully addressed only for nucleoside monophosphates,[3,4] which can be disguised as pronucleotides that contain charge-masking phosphate modifications that undergo removal after delivery into cells.[5–7] However, such an approach is not suitable for (di)nucleoside di- and triphosphates because fully charge-

masked pyrophosphate bonds are chemically unstable and undergo rapid hydrolysis under aqueous conditions. Therefore, alternative approaches have been developed for the delivery of nucleoside oligophosphates into cells, including application of nanogels,[8] nanoparticles,[9] and naturally-inspired or artificial molecular transporters.[10,11] Meier *et al.* have recently developed cell-permeable nucleoside diphosphate and triphosphate pro-drugs (DiPPro and TriPPro, respectively) that carry highly lipophilic masking groups exclusively at the terminal phosphate, which has yielded a significant breakthrough in this field.[12–14] However, the issue of delivering dinucleoside oligophosphates and other structurally related compounds into cells remains largely unaddressed.[15] Here, we explore whether ligand-mediated cellular delivery of dinucleoside oligophosphates can resolve this problem.

As model dinucleotides with highly promising biological activity *in vitro* but limited applications *in vivo* due to permeability issues, we used 7-methylguanosine 5′ cap analogs. 7-Methylguanosine triphosphate is attached to the 5′ end of all eukaryotic messenger RNAs (mRNAs), forming the so called 5′ cap.[16,17] This cap protects mRNA from premature degradation and participates in initiation of translation by interacting with eukaryotic translation initiation factor 4E (eIF4E). eIF4E is one of the components of translation initiation complex eIF4F, which guides ribosome recruitment to mRNA during protein biosynthesis.[18] eIF4E has been found to act as a regulator of cap-dependent translation that strongly affects translation of

[a]*Centre of New Technologies, University of Warsaw Banacha 2c, 02-097 Warsaw, Poland. E-mail: j.jemielity@cent.uw.edu.pl*

[b]*College of Inter-Faculty Individual Studies in Mathematics and Natural Sciences, University of Warsaw, Banacha 2c, 02-097 Warsaw, Poland*

[c]*Division of Biophysics Institute of Experimental Physics, Faculty of Physics University of Warsaw, Pasteura 5, 02-093 Warsaw, Poland. E-mail: jkowalska@fuw.edu.pl*

[d]*Faculty of Biology University of Warsaw, I. Miecznikowa 1, 02-096 Warsaw, Poland*

[e]*Institute of Physical Chemistry Polish Academy of Sciences, Kasprzaka 44/52, 01-224 Warsaw, Poland*

† Electronic supplementary information (ESI) available. See DOI: 10.1039/d1sc02143e

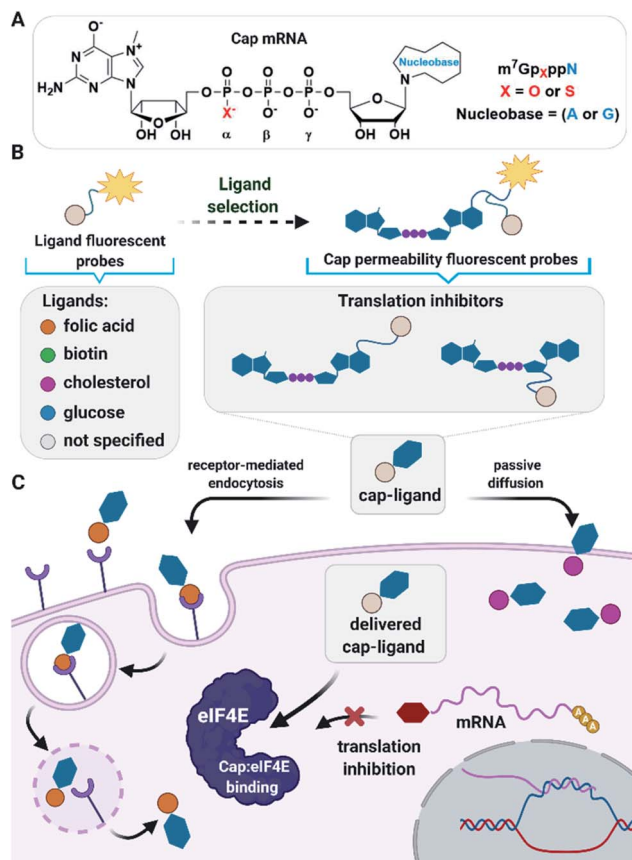‡ These authors contributed equally to this work.

Fig. 1 (A) mRNA 5′ cap structure, (B) ligand selection process methodology using fluorescent probes, (C) mode of action for translation inhibitors (cap-ligands) and their cellular delivery and interaction with eIF4E. The folic acid – receptor-mediated endocytosis pathway and passive diffusion for cholesterol are displayed. Created with https://www.BioRender.com.

selected intracellular mRNAs. These transcripts ("weak" mRNAs) usually have long structured 5′-untranslated regions (UTRs) and, interestingly, many encode proteins responsible for angiogenesis (VEGF-A), cell proliferation (c-myc), cell survival (Bcl-2), and other aspects of oncogenesis.[19] Increased eIF4E expression is associated with poor prognosis in cancer patients[20] and induces cancer transformation of primary epithelial cells and fibroblasts.[21,22] In contrast, downregulation of eIF4E levels inhibits melanoma proliferation and invasion.[23] Therefore, various therapeutic strategies for targeting eIF4E have been proposed to combat carcinogenesis.[24,25] These include antisense oligonucleotides and siRNAs to modulate eIF4E mRNA levels,[26,27] aptamers which target eIF4E,[28,29] and small molecules to disrupt the stability of the eIF4F complex either by preventing eIF4E binding to the mRNA 5′ cap or by hindering association of eIF4E with the eIF4G scaffold protein.[30,31]

Synthetic cap analogs have been studied as potential eIF4E antagonists for nearly three decades,[32] but their activity was limited by poor cell permeability. Of these, 7-alkylaryl 5′-monophosphates were identified as potent eIF4E antagonists. To enable cellular uptake, the compounds have been converted

to several prodrugs including tryptamine phosphoramidates of N7-benzyl GMP (4Ei-1) and 7-Cl-phenylethylene GMP that release active drugs inside cells.[33–35] However, this strategy is applicable only to monophosphorylated cap analogs, which in vitro have much lower activity than their di-, and triphosphate counterparts.[36]

A particularly promising group of cap-derived eIF4E antagonists are oligophosphorylated mono- and dinucleotide cap analogs that have high affinity for eIF4E and are resistant to degradation by the cap-specific pyrophosphatase DcpS.[37,38] Numerous DcpS-resistant dinucleotide cap analogs have been designed by replacing one or more oxygen atoms in the triphosphate bridge with another atom or group of atoms (e.g. compounds carrying non-bridging γ-O-to-S, γ-O-to-BH$_3$, β-O-to-BH$_3$,[39,40] bridging β-γ-O-to-CH$_2$ or β-γ-O-to-NH,[41–43] or 5′-O-to-S [5′-PSL][44]) and have shown superior potency and stability in rabbit reticulocyte lysates. However, the potential use of these compounds has never been demonstrated in vivo.

Here, we sought to develop a ligand-based approach for the delivery of dinucleotide cap analogs into cells that would also be applicable also to other biologically relevant dinucleoside oligophosphates. As potential transporters, we evaluated several small molecule ligands previously identified as transporting vehicles for various types of (macro)biomolecules (Fig. 1). The tested ligands included folic acid, which uses a receptor-mediated endocytosis pathway;[45] biotin, which is dominantly taken up by high-affinity biotin transporters;[46] glucose, which enters cells through facilitated diffusion;[47] and cholesterol, which facilitates passive diffusion of small molecules into cells.[48] To select the most active ligands and ideal cell culture models, we first studied simple fluorescent probes using flow cytometry, confocal microcopy, and fluorescence correlation spectroscopy (FCS). Based on those studies we synthesized several cap analogs decorated with select ligands and a fluorescent dye to verify that the ligands are capable of transporting negatively charged dinucleoside oligophosphates into cells. After confirming the proof of concept, we synthesized a series of cap analogs differing in susceptibility to DcpS and conjugated those to the most potent ligands to examine their biological activity both in vitro and towards breast cancer cells. As a result, we identified several compounds with good cellular permeability, high activity, and stability in vitro, and ability to induce apoptosis in cancer cells.

Results and discussion

Synthesis of fluorescent probes and their permeability assessment

We first verified the ability of select ligands to transport polar molecules into cells and choose optimal cell culture models for further experiments. Probes 1–4 were thus designed consisting of the non-permeable fluorescent dye fluorescein (FAM) conjugated to folic acid, biotin, glucose, or cholesterol via a polyether linker (Fig. 2A).

The probes were synthesized by taking advantage of N-hydroxysuccinimide chemistry (NHS) and previously reported procedures (Fig. 2B and C; ESI†).[49–51] The cellular permeability
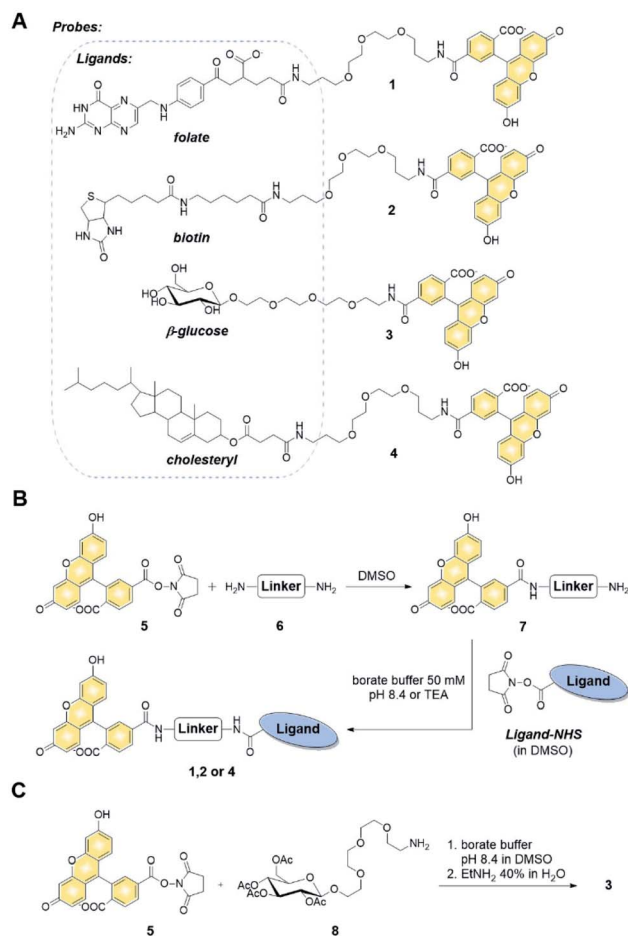
Fig. 2 Chemical synthesis of probes 1–4 (A) structures of probes 1-4, (B) synthesis of compounds 1, 2 and 4 via NHS chemistry: linker: 4,7,10-trioxa-1,13-diaminotridecane (6), ligand-NHS: folate-NHS, biotin-NHS, cholesteryl hemisuccinate-NHS, (C) synthesis of compound 3.
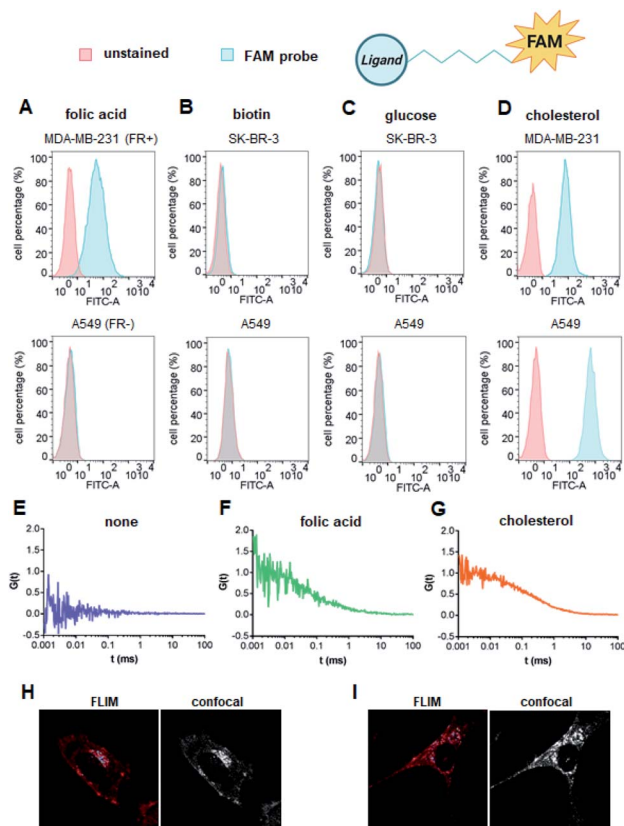

Fig. 3 Initial selection of cell-permeable ligands. (A–D) Specific cell lines were incubated with FAM-labeled probes and their cellular uptake were assessed by flow cytometry. Histograms represent overlaid flow cytometry data as a percentage of unstained and FAM-ligand (50 nM) – stained cells. (A) Probe 1 uptake in MDA-MB-231 cells compared to A549 cells. Probe 2–4 uptake in SK-BR-3 and MDA-MB-231 cells compared to A549 cells, respectively (B–D). Normalized FCS autocorrelation curves obtained in MDA-MB-231 cells incubated with (E) FAM-PEG, probe 1 (F) or 4 (G). Confocal imaging/FLIM of a cell incubated with 50 nM probe 1 (H) or 4 (I). FLIM image colored according to the scheme: blue – fluorescence lifetime < 2.4 ns (autofluorescence), red – fluorescence lifetime > 2.6 ns (probe).

of the probes was evaluated in three human cancer cell lines: MDA-MB-231, which overexpress folate receptor (FR) α for endosomal uptake of folic acid;[52] SK-RB-3, which expresses the SMVT1 receptor for biotin[46] and the GLUT-1 transporter for glucose;[53] and A549, which expresses none of these receptors.[54] Potential uptake of probes 1–4 was initially assessed by flow cytometry. Cells were incubated with the probes for 2 h followed by flow cytometry analysis of the cells to quantify FAM emission. Folic acid-conjugated probe 1 efficiently increased FAM emission of MDA-MB-231 cells, but not A549 cells (Fig. 3A), suggesting that delivery via receptor-mediated endocytosis might occur indeed in the former case. Neither the biotin-conjugated probe 2 nor β-glucose-conjugated probe 3 affected the FAM emission in any of the studied cell lines (Fig. 3B and C). In contrast, the cholesterol-conjugated probe 4 increased FAM emission for all studied cells lines (Fig. 3D), suggesting either internalization via a diffusion-based mechanism or unspecific binding to cell membrane.

To further qualitatively and quantitatively evaluate the uptake of probes 1 and 4 into MDA-MB-231 cells we used FCS

method, which verifies probe localization and estimates the size of fluorescent entities. FCS enables the measurement of the diffusion coefficients for various fluorescently-labeled probes in the cell.[55] By knowing the hydrodynamic radius of the studied probe and employing a cytoplasm viscosity model for various length scales, one can predict the theoretical coefficient for the probe freely diffusing in the cytoplasm and compare it to experimental values.[56–58] If the value measured in the cells is lower than the predicted value, it indicates binding of the probe to the cellular components. To that end, the hydrodynamic radii of probes 1 and 4 (Tables S1 and S2†) and cytoplasmic viscosity of MDA-MB-231 cells were first established by FCS (Table S3 and Fig. S1†).

The cellular uptake of these probes, along with linker-functionalized fluorescein (FAM-PEG), were then studied by FCS. MDA-MB-231 cells were incubated for 1 h with 1, 4, or FAM-PEG and subjected to FCS measurements based on which the autocorrelation curves were calculated (Fig. 3E–G). For

Table 1 Results of FCS measurements in the cytoplasm of MDA–MB-231 cells incubated with fluorescent probes[a]

Probe	FAM-PEG-FA (1)	FAM-PEG-CHOL (4)	m⁷GpppA-FAM-FA (15)	m⁷GpppA-FAM-CHOL (17)
D_{cyto} [$\mu m^2\ s^{-1}$], predicted for free probe in cytosol	187	205	96.6	58.5
D_1 [$\mu m^2\ s^{-1}$], faster component in FCS	184 ± 56	203 ± 29	87.0 ± 43.6	58.2 ± 12.4
D_2 [$\mu m^2\ s^{-1}$], slower component in FCS	1–9 high variability	3–14 high variability	0.1–9.8 high variability	0.1–5 high variability

[a] D_{cyto} – diffusion coefficient in the cytoplasm.

compounds **1** and **4**, FCS autocorrelation curves were fitted with a two-component free diffusion model (Table 1, Table S1†) while for the FAM-PEG probe, no autocorrelation of fluorescence signal was detected. For both probes, the diffusion coefficients for the first, faster component (D_1) were in line with values expected for free diffusion of the probes in cytosol (187 $\mu m^2\ s^{-1}$ and 205 $\mu m^2\ s^{-1}$, respectively, Table 1), whereas the slower components (D_2) showed high variability from 1 $\mu m^2\ s^{-1}$ to 14 $\mu m^2\ s^{-1}$. Such D_2 values are characteristic for large proteins and small membrane structures.

No components with $D < 0.1\ \mu m^2\ s^{-1}$, which is typically interpreted as active transport of endosomes, was observed for any of the probes. To verify localization of probes **1** and **4**, fluorescent lifetime imaging (FLIM) was performed (Fig. 3H and I). FLIM, in contrast to typical confocal microscopy, enables differentiation of emission coming from the probe (characterized by long fluorescence lifetimes, $t > 2.6$ ns) from autofluorescence of the cell ($t < 2.4$ ns). These observations confirmed the presence of compounds **1** and **4** in MDA-MB-231 cells and revealed mostly cytoplasmatic localization for both. Overall, these data indicate that both folic acid and cholesterol are good candidates for studying cap analog delivery into cancer cells. The initial evaluation in different cultured cells suggested that cholesterol-conjugated probe **4** is taken up by a receptor-independent mechanism, whereas uptake of probe **1** requires the presence of folic acid receptors on the cell surface. However,

the FCS measurements did not provide any further details differentiating these two potential mechanisms.

Synthesis of fluorescent cap–ligand conjugates (m⁷GpppA-FAM-ligand) and their cellular permeability

We next tested whether folic acid and cholesterol may facilitate delivery of dinucleotide cap analogs into cells. To that end, we synthesized a series of doubly functionalized cap analogs that were labeled with fluorescein and conjugated to either folic acid, biotin, or cholesterol (**15**, **16**, and **17**, respectively; compound **16** being used as a negative control). The label and ligand were attached at the position N6 of adenine by means of NHS and CuAAC chemistry, respectively, and a multivalent polyamine linker (Scheme 1 and ESI†).

Flow cytometry analysis showed that the cap analog conjugated with folic acid (**15**) potentially penetrated into MDA-MB-231 cells (FR+), but not A549 cells (FR−) (Fig. 4A and B). This is consistent with the results obtained for probe **1**, and reveals that the presence of negative charge in the small molecule does not prevent transport by folic acid receptors.

Compound **17**, bearing the cholesterol moiety, penetrated into both the MDA-MB-231 and A549 cell lines (Fig. 4A and B), which also agrees with the results obtained for probe **4**. As expected, based on the results for probe **2**, neither cell line took up biotin-conjugated compound **16** (Fig. 4A and B).
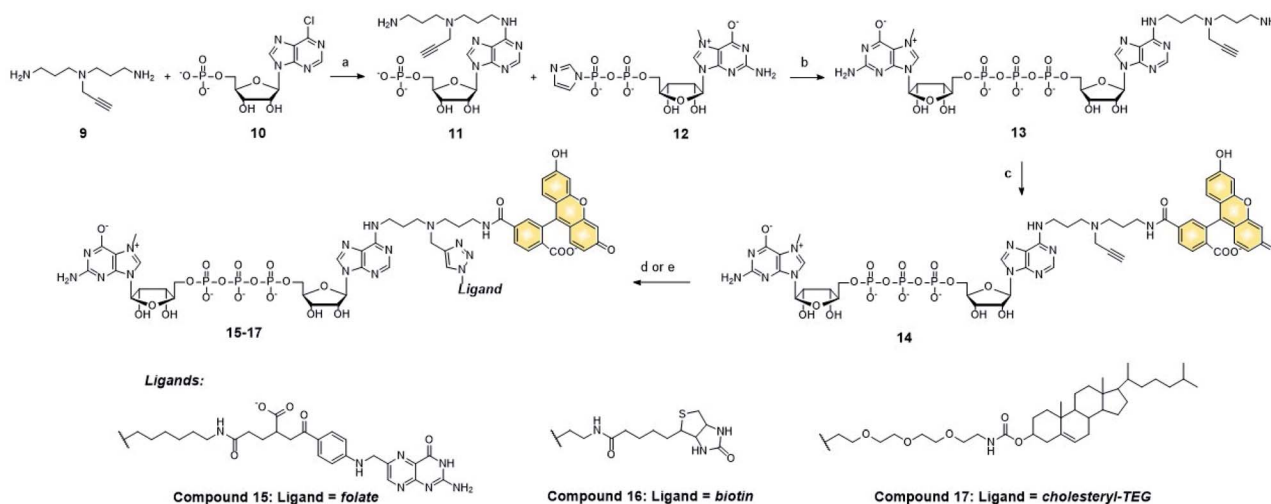
Scheme 1 Chemical synthesis of fluorescently labeled cap conjugates. Conditions and reagents: (a) H₂O, NaOH to adjust to pH = 8, 72 h, 65 °C, (b) ZnCl₂, DMF, 24 h, rt, (c) 6-carboxyfluorescein-N-hydroxysuccinimide (FAM-NHS), borate buffer (50 mM), pH = 8.4, DMSO, (d) for **15** (with folate azide) and **16** (with biotin azide): CuSO₄ x5H₂O, NaAsc, DMSO : H₂O, (e) for **17** (with cholesteryl-TEG-azide): Cu(ɪɪ)-TBTA, NaAsc, triethylammonium acetate pH = 7, DMSO.
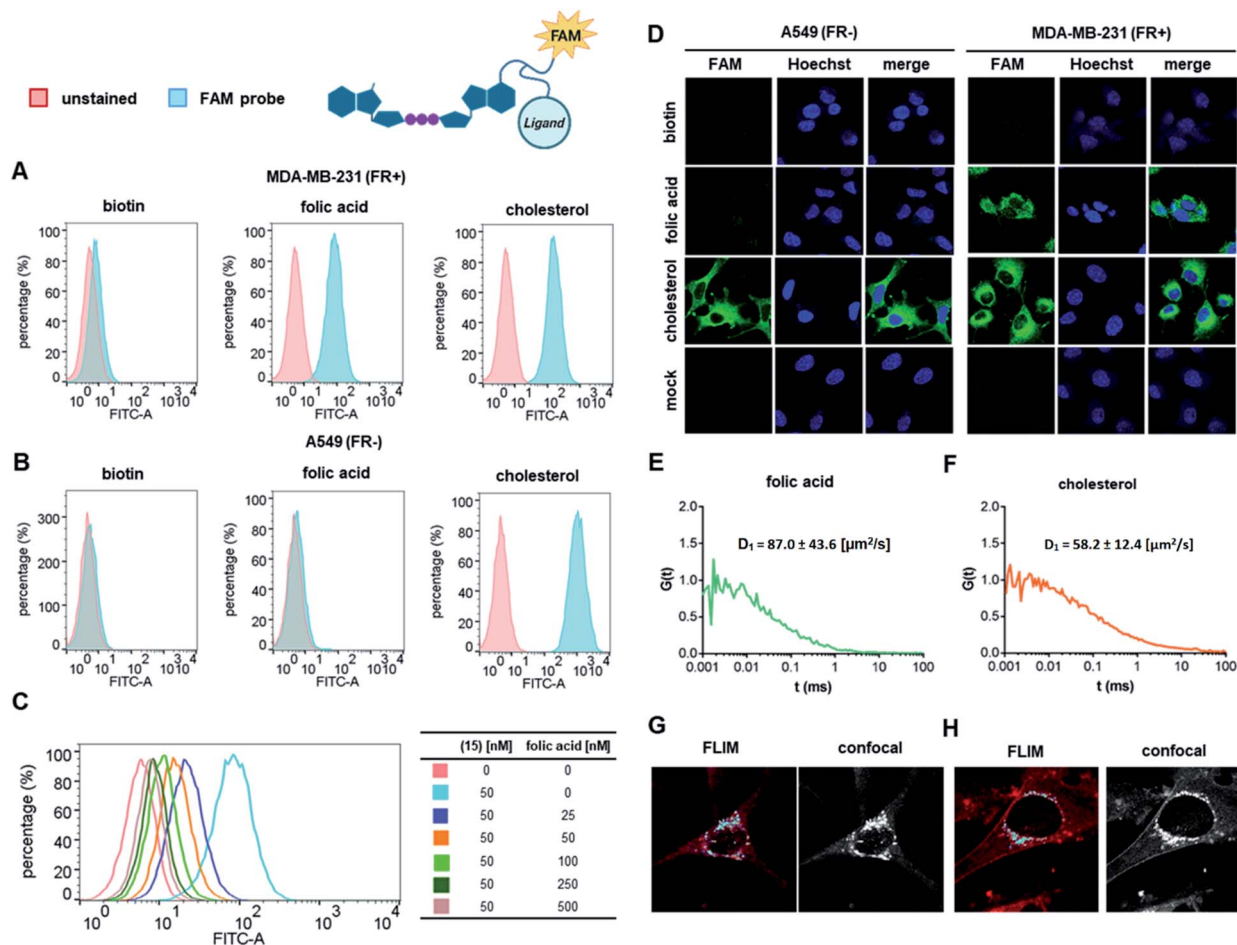
Fig. 4 Cellular uptake of FAM labeled cap analog probes by (A) MDA-MB-231 and (B) A549 cells assessed by flow cytometry. Histograms represent overlaid flow cytometry data of unstained and m^{7}GpppA-FAM-ligand (50 nM)-stained cells. (C) Probe **15** uptake by MDA-MB-231 cells (50 nM) in the presence of increasing concentrations of folic acid. Histograms represent overlaid flow cytometry data as a percentage of unstained and m^{7}GpppA-FAM-FA-stained cells. (D) Uptake of FAM labeled cap analog conjugates by A549 and MDA-MB-231 cells assessed by confocal microscopy. (E and F) Normalized FCS autocorrelation curves for MDA-MB-231 cells incubated with probes **15** and **17** and their diffusion coefficients in cytoplasm derived from FCS data. Confocal imaging/FLIM of a cell incubated with 50 nM probe **15** (H) and **17** (G). FLIM image colored according to the scheme: blue – fluorescence lifetime < 2.4 ns (autofluorescence), red – fluorescence lifetime > 2.6 ns (probe).

To additionally verify that cellular uptake of compound **15** is dependent on FR expression on the cell membrane, we performed a flow-cytometry based competition assay (Fig. 4C). The uptake of compound **15** was inhibited in a dose-dependent manner by free folic acid in the cell culture medium, indicating an FR-specific mechanism. The uptake of compounds **15**, **16**, and **17** was independently studied by confocal microscopy (Fig. 4D) and verified by checking the orthogonal axis views (Fig. S2†). The results were generally consistent with the flow cytometry data, with compound **15** permeating only into MDA-MB-231 (FR+) cells, compound **17** permeating into both cell lines, and compound **16** being non-permeable.

FCS measurements performed in MDA-MB-231 cells (Fig. 4E and F) revealed primarily cytoplasmic localization for both compounds **15** and **17**. The diffusion coefficients (D_1) of the major, faster components were in line with values expected for free diffusion of the probes in the cytosol (Table 1, Table S1†), suggesting that the most abundant fluorescent species in the

cell is a compound successfully delivered to the cytoplasm. The slower components (D_2) showed high variability from 0.1 μm^2 s^{-1} to 9.8 μm^2 s^{-1}, which is characteristic for large proteins and small membrane structures. Components with $D < 0.1$ μm^2 s^{-1}, typically assigned to endosomes, have not been found in the FCS signals for any of the studied probes.

Cap analog conjugates with folic acid and cholesterol inhibit cap-dependent translation *in vitro*

After identifying the ligands capable of transporting the cap analogs into cells, we focused on optimizing the structure of the cap residue to maximize its translation inhibitory properties. In particular, we focused on tailoring the ligand attachment site for optimal interaction with eIF4E and decreasing susceptibility to cleavage by DcpS – the pyrophosphatase that rapidly degrades native cap residues in the cell. Therefore, we synthesized a series of cap analogs carrying amino-alkyl linkers at either the *N*6-position of adenosine or the ribose moiety of
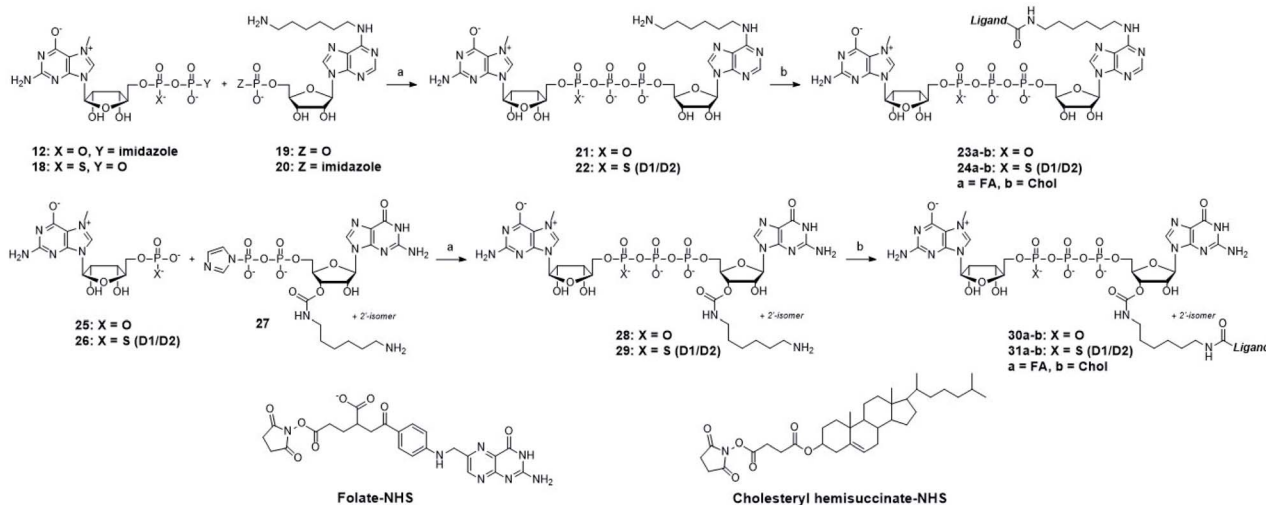
Scheme 2 Chemical syntheses and applied conditions and reagents: (a) $ZnCl_2$, DMF, (b) NHS-activated ligand (a = FA – folate, b = Chol – cholesteryl hemisuccinate), borate buffer pH = 8.4, DMSO. Phosphorothioates (**18**, **22**, **24**, **26**, **29**, **31**) were obtained as a mixture of diastereoisomers (D1/D2).

guanosine and optionally introduced a γ-phosphorothioate (γ-PS) modification that prevents the cleavage by DcpS[40] (compounds **21**, **22**, **28**, and **29**, Scheme 2). Phosphorothioate cap analogs (**22**, **29**) exist as two *P*-diastereomers (D1/D2) that were difficult to separate by RP HPLC. Since the initial results showed that the affinities of the diastereomers for eIF4E were very similar (Fig. S3†), we decided to use diastereomeric mixtures of **22** and **29** in further studies.

Folic acid or cholesterol were then attached to these cap analogs using NHS-chemistry[47,48] to obtain eight different cap–ligand conjugates (**23a–b**, **24a–b**, **30a–b**, and **31a–b**). The conjugates were purified by RP HPLC and their *m/z* values were confirmed by high-resolution mass spectrometry (HR-MS, ESI†).

We next assessed the affinity of these conjugates to eIF4E. To this end, a recently developed fluorescence intensity binding assay based on a pyrene-labeled probe (PyFLINT-B) was applied.[59] The PyFLINT-B assay is based on measuring changes of pyrene fluorescence in a pyrene-labeled probe upon its competitive displacement from eIF4E by the studied compounds and allows for fast and reliable measurement of apparent dissociation constants, based on which equilibrium dissociation constants (K_D) can be calculated. The K_D values of all studied ligands, along with the reference compounds m^7GpppA and m^7GpppG, are shown in Table 2, while the binding curves are shown in the ESI (Fig. S2†). The affinity of m^7GpppG for eIF4E as determined by PyFLINT-B was 2-fold

Table 2 Biological properties of synthetized cap analogs

No.	Compound	$K_D{}^a$ [μM]	IC_{50} [μM] (translation inhibition)^b	IC_{50} [μM] (cytotoxicity)^c
21	m^7GpppA	0.429 ± 0.079	$78. \pm 26$	≫30
	m^7GpppA-HDA	0.884 ± 0.148	23.9 ± 5.5	nd.
22	m^7Gp$_S$ppA-HDA-D1/D2	0.433 ± 0.102	10.8 ± 1.7	nd.
23a	m^7GpppA-HDA-FA	0.39 ± 0.09	28.1 ± 4.2	≫ 30
23b	m^7GpppA-HDA-CHOL	0.051	12.6 ± 2.1	8.28 ± 1.87
24a	m^7Gp$_S$ppA-HDA-FA D1/D2	0.30 ± 0.06	29.9 ± 3.3	≫30
24b	m^7Gp$_S$ppA-HDA-CHOL D1/D2	nd.^{e}	nd.^{e}	5.20 ± 0.78
	m^7GpppG	0.216 ± 0.035	39.6 ± 13.7	≫30
28	m^7GpppG-L$_{6N}$-2′-*O*/3′-*O*	0.485 ± 0.092	10.9 ± 1.4	nd.
29	m^7Gp$_S$ppG-L$_{6N}$-2′-*O*/3′-*O* D1/D2	0.242 ± 0.045	6.0 ± 0.8	nd.
30a	m^7GpppG-L$_{6N}$ -2′-*O*/3′-*O*-FA	0.12 ± 0.02	16.1 ± 3.5	≫30
30b	m^7GpppG-L$_{6N}$ -2′-*O*/3′-*O*-CHOL	0.043	26.1 ± 5.0	10.90 ± 2.81
31a	m^7Gp$_S$ppG-L$_{6N}$ -2′-*O*/3′-*O*-FA D1/D2	0.10 ± 0.02	4.2 ± 0.6	≫30
31b	m^7Gp$_S$ppG- L$_{6N}$ 2′-*O*/3′-*O*-CHOL D1/D2	0.026	20.5 ± 5.7	6.52 ± 1.73 μM $[6.04 \pm 1.58]^d$
	Folic acid	>10	≫500	≫30
	Cholesterol	0.94	$99. \pm 20.$	≫30

^{a} Dissociation constants (K_D) for eIF4E–cap analog complexes determined using the PyFLINT-B method at 20 °C. Data shown are means ± SD of three independent experiments; for compounds **23b**, **30b**, and **31b**, only one repetition was performed. ^{b} From cap-dependent translation inhibition in rabbit reticulocyte lysate (RRL). ^{c} From resazurin cell viability assay in MDA-MB-231 cells. ^{d} Value in brackets is for K562 cells. ^{e} The values were not determined due to limited available material.

higher than that of m[7]GpppA, which is in agreement with previous findings by other methods.[60] The introduction of an aminohexyl linker at the $N6$ position of adenosine (compound **21**) resulted in about 2-fold decrease in affinity for eIF4E (K_D 0.88 ± 0.15 μM for m[7]GpppA-HDA (**21**) *vs.* K_D 0.43 ± 0.08 μM for m[7]GpppA). A similar thermodynamic effect was observed upon introduction of the linker at the ribose moiety of guanosine (compound **28**) (K_D 0.485 ± 0.092 μM for m[7]GpppG-L$_{6N}$ (**28**) *vs.* K_D 0.216 ± 0.035 μM for m[7]GpppG).

The presence of the γ-PS moiety increased affinity to eIF4E by about 2-fold (K_D 0.88 ± 0.15 μM for m[7]GpppA-HDA (**21**) *vs.* K_D 0.43 ± 0.10 μM for m[7]Gp$_S$ppA-HDA D1/D2 (**22**) and K_D 0.485 ± 0.092 μM for m[7]GpppG-L$_{6N}$ (**28**) *vs.* K_D 0.242 ± 0.045 μM for m[7]Gp$_S$ppG-L$_{6N}$-2′-O/3′-O D1/D2 (**29**)). Interestingly, the introduction of appropriate ligands (FA or Chol; compounds **23a** to **31b**) alleviated the destabilizing effect introduced by the aminoalkyl linker, suggesting it was at least partly caused by electrostatic repulsion of the positively charged amino group with positively charged surfaces in eIF4E. K_D values for compounds bearing the folate modification were from 1.5-fold to 4-fold higher than corresponding unconjugated caps (*e.g.* K_D 0.433 ± 0.102 μM for m[7]Gp$_S$ppA-HDA-D1/D2 (**22**) *vs.* K_D 0.30 ± 0.06 μM for m[7]Gp$_S$ppA-HDA-FA D1/D2 (**24a**)). Unexpectedly, the incorporation of the cholesterol moiety resulted in even greater stabilization of the cap-eIF4E complex ranging from 9-fold to 17-fold improvement (*e.g.* K_D 0.242 ± 0.045 μM for m[7]Gp$_S$ppG-L$_{6N}$-2′-O/3′-O D1/D2 (**29**) *vs.* K_D 0.026 μM for m[7]Gp$_S$ppG-L$_{6N}$-2′-O/3′-O-CHOL D1/D2 (**31b**)). This might be due to additional hydrophobic interactions with eIF4E provided by the cholesteryl moiety.

In order to evaluate the ability of cap analogs to target eIF4E in a more complex biological system, we studied their potency to inhibit cap-dependent translation in rabbit reticulocyte lysate (RRL) programmed with capped luciferase-encoding mRNA.[61] We have previously shown that the ability of cap analogs to inhibit translation in RRL correlates qualitatively with their affinity for eIF4E, but may also be affected by DcpS-like activity, which is also present in the lysate.[62] Therefore, the compounds were tested in an experimental set up in which both factors could be taken into account. Namely, the compounds were incubated in RRL for 1 h followed by the addition of mRNA and luciferase activity measurement after another hour. It was expected that 1 h pre-incubation in RRL will relatively decrease the inhibitory potency of cap analogs susceptible to DcpS, compared to analogs that are resistant to DcpS.[62]

The IC$_{50}$ values reasonably correlated with K_D values from PyFLINT-B assay (Table 2), albeit with some important exceptions. For instance, the introduction of hexamine linkers resulted in stronger inhibition compared to unmodified reference compounds [IC$_{50}$ 23.9 ± 5.5 μM for m[7]GpppA-HDA (**21**) *vs.* IC$_{50}$ 78.1 ± 25.6 μM for m[7]GpppA and IC$_{50}$ 10.9 ± 1.4 μM for m[7]GpppG-L$_{6N}$ (**28**) *vs.* IC$_{50}$ 39.6 ± 13.7 μM for m[7]GpppG; Table 2, Fig. S4],† despite their lower affinity for eIF4E. This observation confirms that factors other than affinity for eIF4E, and DcpS-susceptibility in particular, influence the inhibitory properties under the conditions of our experiment. DcpS exhibits a tight cap-binding mode,

consequently affinity and susceptibility of cap analogs to DcpS is usually decreased upon functionalization of ribose or nucleobase moieties.[40,63,64]

Therefore, it is plausible that the incorporation of a linker at the $N6$-position of adenine or the 2′-O/3′-O-position of ribose in the cap decreased its susceptibility to DcpS, thereby stabilizing it in the lysate. The presence of γ-PS conferred high inhibitory potency for all tested compounds. Compounds **22** and **29** bearing this modification had lower IC$_{50}$ values than their unmodified counterparts (IC$_{50}$ 23.9 ± 5.5 μM for m[7]GpppA-HDA (**21**) *vs.* IC$_{50}$ 10.8 ± 1.7 μM for m[7]Gp$_S$ppA-HDA D1/D2 (**22**) and IC$_{50}$ 10.9 ± 1.4 μM for m[7]GpppG-L$_{6N}$ (**28**) *vs.* IC$_{50}$ 6.0 ± 0.8 μM for m[7]Gp$_S$ppG-L$_{6N}$-2′-O/3′-O D1/D2 (**29**)). This observation is in agreement with our previous studies showing that a non-bridging γ-O-to-S modification in the triphosphate bridge decreases the susceptibility of cap analogs to DcpS (in addition to stabilizing the cap-eIF4E complex).[40] Interestingly, despite a significant increase in affinity for eIF4E, the presence of ligands did not enhance inhibitory properties of cap analogs in RRL compared to corresponding compounds with aminohexyl linkers. Compounds **23a**, **23b**, **30a**, and **31a** had IC$_{50}$ values almost unchanged compared to values for the cap analogs with aminoalkyl linkers, whereas compounds **24a**, **30b**, and **31b** were up to 3-fold weaker inhibitors. Overall, all cap–ligand conjugates studied exhibited sufficient potency and stability in RLL to be considered as suitable candidates for evaluation in cell culture experiments.

Cholesterol cap analogs influence cell viability and their potency depends on a 5′,5′-triphosphate bridge modification

Knowing the *in vitro* properties of the synthesized conjugates, we next analyzed their cytotoxicity towards a breast cancer cell line (MDA-MB-231). We first verified whether the non-fluorescent cap analogs entered the cells. To that end, an immunofluorescent assay using a cap-specific antibody was employed.[10] Visualization of immunostained cells clearly showed that cap analog conjugates were taken up by MDA-MB-231 (FR+) cells regardless of the attached ligand (Fig. 5A).

Next, cytotoxicity of the compounds (**23a**, **23b**, **24a**, **24b**, **30a**, **30b**, **31a**, **31b**, m[7]GpppA, m[7]GpppG, free folic acid, and free cholesterol moiety) towards MDA-MB-231 cells was determined by resazurin assay. Only the cholesterol conjugates significantly influenced cell viability (Fig. 5B and S5†). The compounds carrying the γ-PS moiety in the 5′,5′-triphosphate bridge (**24b** and **31b**) had cytotoxic effects about 2-fold stronger than unmodified counterparts (IC$_{50}$ 8.3 ± 1.9 μM for **23b** *vs.* IC$_{50}$ 5.2 ± 0.8 μM for **24b** and IC$_{50}$ 10.9 ± 2.8 μM for **30b** *vs.* IC$_{50}$ 6.0 ± 1.6 μM for **31b**), clearly showing that stabilizing the cap against DcpS is beneficial for the biological activity of the cap analogs in living cells (Fig. 5C). Next, we checked whether cholesterol cap analogs exhibit cytotoxic activity towards other cancer cell lines. To that end, a leukemia cancer cell line (K562) was treated with cap analog **31b**. Resazurin assay confirmed the cytotoxicity of this compound towards the K562 cell line (Fig. 5D; IC$_{50}$ 6.5 ± 1.7 μM) at a level comparable to MDA-MB-231 cells (IC$_{50}$ 6.0 ± 1.6 μM; Table 2).
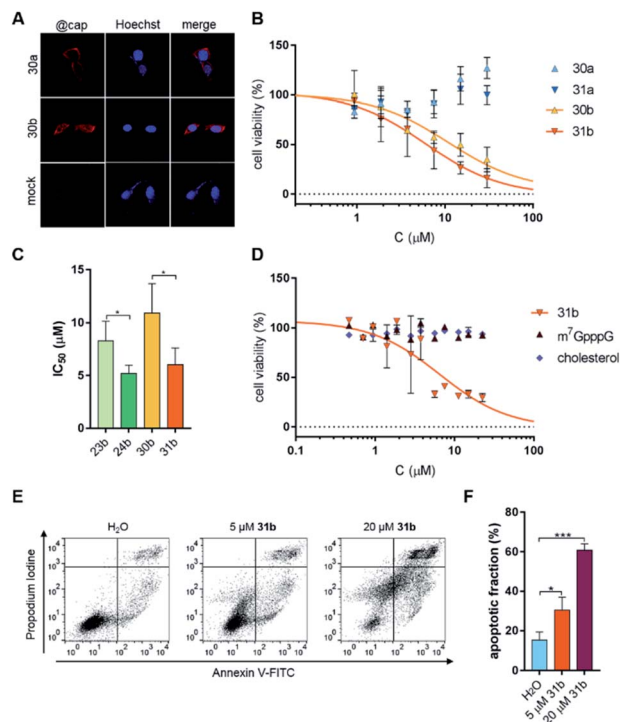
Fig. 5 Cellular response to cap analog conjugates. (A) Verification of cellular delivery of cap conjugates. MDA-MB-231 cells after 2 h treatment with 0.5 µM compound were fixed and stained with anti-cap antibody. (B) Viability of MDA-MB-231 cells treated with different concentrations of selected compounds. After 72 h incubation, cells viability was assessed with the resazurin assay. Data points were normalized to mock treated cells for each time point and represent mean value ± SD from at least two independent biological replications with two technical replicates per treatment. (C) IC_{50} values of cholesterol cap analog conjugates calculated based on the cell viability assay presented in (B), bars represent mean value ± SD. Statistical significance: * $p < 0.05$, ** $p < 0.01$ (Welch's t test). (D) Viability of K562 cells treated with different concentrations of selected compounds. After 72 h incubation, cells viability was assessed with the resazurin assay. Data points were normalized to mock treated cells for each time point and represent mean value ± SD two independent biological replications with two technical replicates per treatment. (E) Apoptosis assessed by Annexin V/propidium iodide staining. K562 cells were treated with 5 µM and 20 µM **31b** for 20 h and examined by flow cytometry. Viable cells are in the (I) lower left quadrant, early apoptotic are in the (II) lower right quadrant, late apoptotic cells are in the (III) upper right quadrant and non-viable necrotic cells are in the (IV) upper left quadrant. (F) Apoptotic cell fraction calculated based on the Annexin V/propidium iodide staining presented in (E). Bars represent mean value ± SD from at least three independent biological replications. Statistical significance: * $p < 0.05$, *** $p < 0.001$ (Welch's t test).

Cholesterol cap analogs induce apoptosis in a leukemia cell line

Most anticancer drugs currently used in clinical oncology exploit apoptotic mechanisms to trigger cancer cell death.[65] Therefore, to verify whether cholesterol-conjugated cap analogs induce apoptosis in cancer cells, K562 cells were incubated with the most potent compound (**31b**), followed by a more detailed cell viability analysis. The ability of **31b** to induce apoptosis was determined by flow cytometry using Annexin V and PI

(propidium iodide) staining. This analysis detects changes in plasma membrane integrity during cell apoptosis that result in the appearance of phosphatidylserine on the outer leaflet of the membrane.

Annexin V has a strong, calcium-dependent affinity for phosphatidylserine and, therefore, can be used as a marker of apoptosis. PI is a DNA binder and can be used to detect genomic DNA released from necrotic cells. Double staining with PI and Annexin V enables differentiation and quantification of living, apoptotic, and necrotic cells. Fig. 5E shows representative dot plots from Annexin V/PI staining, whereas Fig. 5F shows the percentages of apoptotic cells. These data reveal that compound **31b** indeed induces apoptosis in a dose-dependent manner (30.5 ± 6.5% and 60.8 ± 3.2% apoptosis in the presence 5 µM and 20 µM cap analog, respectively).

Conclusions

We synthesized a series of fluorescent probes and doubly functionalized cap analogs, which allowed us to examine the potential of four pre-selected ligands (folic acid, biotin, glucose, and cholesterol) to transport polar, negatively charged molecules into cells. Only folic acid and cholesterol facilitated cellular uptake of fluorescent probes and cap analogs in the studied models. The lack of observable cellular uptake for glucose and biotin conjugates may result from insufficient transport efficiency for these ligands in the studied cell lines or disturbance of the transport by cargo attachment.

We next optimized the structure of the cap moiety for conjugation with folic acid and cholesterol to maximize its translation inhibitory properties. To that end, we synthesized a set of cap-derived eIF4E antagonists with folic acid and cholesterol attached in two different positions of cap analogs (at the nucleobase and the ribose moiety) and optionally carrying a γ-PS modification that prevents cap degradation by DcpS. We tested the cytotoxicity of these compounds towards cancer cells. Both cholesterol and folate conjugates were efficiently taken up by cancer cells, but cytotoxic effects were only observed for compounds conjugated with cholesterol. The cytotoxicity of these conjugates was notably enhanced by introducing the γ-PS modification in the 5′,5′-triphosphate bridge. The possible explanations of this phenomenon include either strong specific binding to folic acid receptors and resulting entrapment of the cap analogs in residual endosomal structures or competitive binding of the conjugates to other folate recognizing proteins, which prevents binding by eF4E. If this is the case, the issue may be resolved in the future by application of cleavable conjugates that release free cap structures following cell entry. Moreover, the designed cap analogs can serve as a platform to test the potential of other ligands to deliver impermeable compounds to mammalian cells. Importantly, dual labeling of cap analogs enables not only intracellular visualization and tracking but also opens up new possibilities to test combinations of cell penetrating ligands, which could lead to the development of superior delivery strategies such as a dual labeling approach that could bypass the "endosome escape" issue. Further studies, including *in vivo* evaluation on animal

models, are required to fully assess the anticancer activity and selectivity of cap–cholesterol conjugates.

Data availability

All data needed to evaluate the conclusions are present in the paper and in the associated supplementary material.

Author contributions

JK, JJ, NK, and PJS designed the study. NK and ZW performed the syntheses. PJS, NB, and LM performed biological assays. RK performed the binding assay. KK, AK, JM, RH performed FCS and FLIM studies. NK, PS, JK, and JJ prepared the first draft of the manuscript. All authors reviewed, edited, and approved the final version of the manuscript.

Conflicts of interest

There are no conflicts to declare.

Acknowledgements

Notes and references

1 M. K. Yates and K. L. Seley-Radtke, *Antiviral Res.*, 2019, **162**, 5–21.

2 J. Lipfert, S. Doniach, R. Das and D. Herschlag, *Annu. Rev. Biochem.*, 2014, **83**, 813–841.

3 C. Meier, M. Lorey, E. De Clercq and J. Balzarini, *J. Med. Chem.*, 1998, **41**, 1417–1427.

4 I. Lefebvre, C. Perigaud, A. Pompon, A.-M. Aubertin, J.-L. Girardet, A. Kirn, G. Gosselin and J.-L. Imbach, *J. Med. Chem.*, 1995, **38**, 3941–3950.

5 U. Pradere, E. C. Garnier-Amblard, S. J. Coats, F. Amblard and R. F. Schinazi, *Chem. Rev.*, 2014, **114**, 9154–9218.

6 F. Pertusat, M. Serpi and C. McGuigan, *Antivir. Chem. Chemother.*, 2012, **22**, 181–203.

7 A. Kraszewski, M. Sobkowski and J. Stawinski, *Front. Chem.*, 2020, **8**, 595738.

8 S. Vinogradov, A. Zeman, E. Batrakova and A. Kabanov, *J. Controlled Release*, 2005, **107**, 143–157.

9 H. Hillaireau, T. Le Doan, M. Appel and P. Couvreur, *J. Controlled Release*, 2006, **116**, 346–352.

10 M. Zochowska, A.-C. Piguet, J. Jemielity, J. Kowalska, E. Szolajska, J.-F. Dufour and J. Chroboczek, *Nanomedicine*, 2015, **11**, 67–76.

11 Z. Zawada, A. Tatar, P. Mocilac, M. Buděšínský and T. Kraus, *Angew. Chem., Int. Ed.*, 2018, **57**, 9891–9895.

12 C. Meier, *Antiviral Chem. Chemother.*, 2017, **25**, 69–82.

13 T. Gollnest, T. D. de Oliveira, D. Schols, J. Balzarini and C. Meier, *Nat. Commun.*, 2015, **6**, 8716.

14 S. Warnecke and C. Meier, *J. Org. Chem.*, 2009, **74**, 3024–3030.

15 S. F. Dowdy, *Nat. Biotechnol.*, 2017, **35**, 222–229.

16 J. D. Lewis and E. Izaurflde, *Eur. J. Biochem.*, 1997, **247**, 461–469.

17 M. Warminski, P. J. Sikorski, J. Kowalska and J. Jemielity, *Top. Curr. Chem.*, 2017, **375**, 16.

18 A. Batool, S. Aashaq and K. I. Andrabi, *J. Cell. Biochem.*, 2019, **120**, 14201–14212.

19 S. Uttam, C. Wong, T. J. Price and A. Khoutorsky, *Front. Genet.*, 2018, **9**, 470.

20 B. Culjkovic and K. L. Borden, *J. Oncol.*, 2009, **2009**, 1–12.

21 A. Lazaris-Karatzas, K. S. Montine and N. Sonenberg, *Nature*, 1990, **345**, 544–547.

22 S. Avdulov, S. Li, V. Michalek, D. Burrichter, M. Peterson, D. M. Perlman, J. C. Manivel, N. Sonenberg, D. Yee, P. B. Bitterman and V. A. Polunovsky, *Cancer Cell*, 2004, **5**, 553–563.

23 C. E. Joyce, A. G. Yanez, A. Mori, A. Yoda, J. S. Carroll and C. D. Novina, *Cancer Res.*, 2017, **77**, 613–622.

24 J. Chu and J. Pelletier, *Cold Spring Harbor Perspect. Biol.*, 2017, **10**, a032995.

25 A. Fan and P. P. Sharp, *J. Med. Chem.*, 2021, **64**, 2436–2465.

26 J. R. Graff, B. W. Konicek, T. M. Vincent, R. L. Lynch, D. Monteith, S. N. Weir, P. Schwier, A. Capen, R. L. Goode, M. S. Dowless, Y. Chen, H. Zhang, S. Sissons, K. Cox, A. M. McNulty, S. H. Parsons, T. Wang, L. Sams, S. Geeganage, L. E. Douglass, B. L. Neubauer, N. M. Dean, K. Blanchard, J. Shou, L. F. Stancato, J. H. Carter and E. G. Marcusson, *J. Clin. Invest.*, 2007, **117**, 2638–2648.

27 F. Zhou, M. Yan, G. Guo, F. Wang, H. Qiu, F. Zheng, Y. Zhang, Q. Liu, X. Zhu and L. Xia, *Med. Oncol.*, 2011, **28**, 1302–1307.

28 W. M. Guo, K. W. Kong, C. J. Brown, S. T. Quah, H. L. Yeo, S. Hoon and Y. Seow, *Mol. Ther.–Nucleic Acids*, 2014, **3**, e217.

29 S. Miyakawa, *RNA*, 2006, **12**, 1825–1834.

30 N. J. Moerke, H. Aktas, H. Chen, S. Cantel, M. Y. Reibarkh, A. Fahmy, J. D. Gross, A. Degterev, J. Yuan, M. Chorev, J. A. Halperin and G. Wagner, *Cell*, 2007, **128**, 257–267.

31 R. Cencic, D. R. Hall, F. Robert, Y. Du, J. Min, L. Li, M. Qui, I. Lewis, S. Kurtkaya, R. Dingledine, H. Fu, D. Kozakov, S. Vajda and J. Pelletier, *Proc. Natl. Acad. Sci. U. S. A.*, 2011, **108**, 1046–1051.

32 E. Darzynkiewicz, I. Ekiel, S. M. Tahara, L. S. Seliger and A. J. Shatkin, *Biochemistry*, 1985, **24**, 1701–1707.

33 Z. Ahmad, B. A. Jacobson, M. W. McDonald, N. Vattendahl Vidal, G. Vattendahl Vidal, S. Chen, M. Dillenburg, A. M. Okon, M. R. Patel, C. R. Wagner and R. A. Kratzke, *Cancer Chemother. Pharmacol.*, 2020, **85**, 425–432.

34 C. R. Wagner, V. V. Iyer and E. J. McIntee, *Med. Res. Rev.*, 2000, **20**, 417–451.

35 B. Ghosh, A. O. Benyumov, P. Ghosh, Y. Jia, S. Avdulov, P. S. Dahlberg, M. Peterson, K. Smith, V. A. Polunovsky, P. B. Bitterman and C. R. Wagner, *ACS Chem. Biol.*, 2009, **4**, 367–377.

36 J. Zuberek, J. Jemielity, A. Jablonowska, J. Stepinski, M. Dadlez, R. Stolarski and E. Darzynkiewicz, *Biochemistry*, 2004, **43**, 5370–5379.

37 M. Ziemniak, M. Strenkowska, J. Kowalska and J. Jemielity, *Future Med. Chem.*, 2013, **5**, 1141–1172.

38 M. Kalek, J. Jemielity, Z. M. Darzynkiewicz, E. Bojarska, J. Stepinski, R. Stolarski, R. E. Davis and E. Darzynkiewicz, *Bioorg. Med. Chem.*, 2006, **14**, 3223–3230.

39 J. Kowalska, A. Wypijewska del Nogal, Z. M. Darzynkiewicz, J. Buck, C. Nicola, A. N. Kuhn, M. Lukaszewicz, J. Zuberek, M. Strenkowska, M. Ziemniak, M. Maciejczyk, E. Bojarska, R. E. Rhoads, E. Darzynkiewicz, U. Sahin and J. Jemielity, *Nucleic Acids Res.*, 2014, **42**, 10245–10264.

40 J. Kowalska, M. Lewdorowicz, J. Zuberek, E. Grudzien-Nogalska, E. Bojarska, J. Stepinski, R. E. Rhoads, E. Darzynkiewicz, R. E. Davis and J. Jemielity, *RNA*, 2008, **14**, 1119–1131.

41 A. M. Rydzik, M. Kulis, M. Lukaszewicz, J. Kowalska, J. Zuberek, Z. M. Darzynkiewicz, E. Darzynkiewicz and J. Jemielity, *Bioorg. Med. Chem.*, 2012, **20**, 1699–1710.

42 J. Jemielity, J. Kowalska, A. M. Rydzik and E. Darzynkiewicz, *New J. Chem.*, 2010, **34**, 829.

43 A. M. Rydzik, M. Warminski, P. J. Sikorski, M. R. Baranowski, S. Walczak, J. Kowalska, J. Zuberek, M. Lukaszewicz, E. Nowak, T. D. W. Claridge, E. Darzynkiewicz, M. Nowotny and J. Jemielity, *Nucleic Acids Res.*, 2017, **45**, 8661–8675.

44 B. A. Wojtczak, P. J. Sikorski, K. Fac-Dabrowska, A. Nowicka, M. Warminski, D. Kubacka, E. Nowak, M. Nowotny, J. Kowalska and J. Jemielity, *J. Am. Chem. Soc.*, 2018, **140**, 5987–5999.

45 Y. Lu and P. S. Low, *Adv. Drug Delivery Rev.*, 2012, **64**, 342–352.

46 W. X. Ren, J. Han, S. Uhm, Y. J. Jang, C. Kang, J.-H. Kim and J. S. Kim, *Chem. Commun.*, 2015, **51**, 10403–10418.

47 E. C. Calvaresi and P. J. Hergenrother, *Chem. Sci.*, 2013, **4**, 2319.

48 D. Irby, C. Du and F. Li, *Mol. Pharm.*, 2017, **14**, 1325–1338.

49 M. Warminski, P. J. Sikorski, Z. Warminska, M. Lukaszewicz, A. Kropiwnicka, J. Zuberek, E. Darzynkiewicz, J. Kowalska and J. Jemielity, *Bioconjugate Chem.*, 2017, **28**, 1978–1992.

50 A. F. Trindade, R. F. M. Frade, E. M. S. Maçôas, C. Graça, C. A. B. Rodrigues, J. M. G. Martinho and C. A. M. Afonso, *Org. Biomol. Chem.*, 2014, **12**, 3181–3190.

51 S. C. Kinsky, J. E. Loader and A. L. Benson, *J. Immunol. Methods*, 1983, **65**, 295–306.

52 J. D. Seitz, J. G. Vineberg, E. Herlihy, B. Park, E. Melief and I. Ojima, *Bioorg. Med. Chem.*, 2015, **23**, 2187–2194.

53 R. L. Aft, F. W. Zhang and D. Gius, *Br. J. Cancer*, 2002, **87**, 805–812.

54 D. Ren, F. Kratz and S.-W. Wang, *Biochem. Eng. J.*, 2014, **89**, 33–41.

55 R. Macháň and T. Wohland, *FEBS Lett.*, 2014, **588**, 3571–3584.

56 T. Kalwarczyk, N. Ziębacz, A. Bielejewska, E. Zaboklicka, K. Koynov, J. Szymański, A. Wilk, A. Patkowski, J. Gapiński, H.-J. Butt and R. Hołyst, *Nano Lett.*, 2011, **11**, 2157–2163.

57 T. Kalwarczyk, K. Kwapiszewska, K. Szczepanski, K. Sozanski, J. Szymanski, B. Michalska, P. Patalas-Krawczyk, J. Duszynski and R. Holyst, *J. Phys. Chem. B*, 2017, **121**, 9831–9837.

58 K. Kwapiszewska, T. Kalwarczyk, B. Michalska, K. Szczepański, J. Szymański, P. Patalas-Krawczyk, T. Andryszewski, M. Iwan, J. Duszyński and R. Hołyst, *Sci. Rep.*, 2019, **9**, 5906.

59 R. Kasprzyk, B. J. Starek, S. Ciechanowicz, D. Kubacka, J. Kowalska and J. Jemielity, *Chem. -Eur. J.*, 2019, **25**, 6728–6740.

60 A. Niedzwiecka, J. Marcotrigiano, J. Stepinski, M. Jankowska-Anyszka, A. Wyslouch-Cieszynska, M. Dadlez, A.-C. Gingras, P. Mak, E. Darzynkiewicz, N. Sonenberg, S. K. Burley and R. Stolarski, *J. Mol. Biol.*, 2002, **319**, 615–635.

61 J. Jemielity, T. Fowler, J. Zuberek, J. Stepinski, M. Lewdorowicz, A. Niedzwiecka, R. Stolarski, E. Darzynkiewicz and R. E. Rhoads, *RNA*, 2003, **9**, 1108–1122.

62 J. Kowalska, M. Lukaszewicz, J. Zuberek, M. Ziemniak, E. Darzynkiewicz and J. Jemielity, *Bioorg. Med. Chem. Lett.*, 2009, **19**, 1921–1925.

63 M. Gu, C. Fabrega, S.-W. Liu, H. Liu, M. Kiledjian and C. D. Lima, *Mol. Cell*, 2004, **14**, 67–80.

64 A. Wypijewska del Nogal, M. D. Surleac, J. Kowalska, M. Lukaszewicz, J. Jemielity, M. Bisaillon, E. Darzynkiewicz, A. L. Milac and E. Bojarska, *FEBS J.*, 2013, **280**, 6508–6527.

65 G. Pistritto, D. Trisciuoglio, C. Ceci, A. Garufi and G. D'Orazi, *Aging*, 2016, **8**, 603–619.